THE ASTROPHYSICAL JOURNAL, 514:441–447, 1999 March 20

SLOW MAGNETOSONIC WAVES IN CORONAL PLUMES

L. OFMAN
Raytheon ITSS; and NASA Goddard Space Flight Center, Code 682, Greenbelt, MD 20771
V. M. NAKARIAKOV
School of Mathematics and Computational Sciences, University of St. Andrews, St. Andrews, Fife KY 16 9SS, Scotland, UK
AND
C. E. DEFOREST
Stanford University; and NASA Goddard Space Flight Center, Code 682, Greenbelt, MD 20771
Received 1998 September 23; accepted 1998 October 29

ABSTRACT

Recent observations of polar plumes in the southern solar coronal hole by the Extreme-Ultraviolet Imaging Telescope (EIT) on board the *SOHO* spacecraft show signatures of quasi-periodic compressional waves with periods of 10–15 minutes. The relative wave amplitude was found to increase with height in the plumes up to about 1.2 $R_\odot$. Using a one-dimensional linear wave equation for the magnetosonic wave, we show that the waves are propagating and that their amplitude increases with height. The observed propagation velocity agrees well with the expected sound velocity inside the plumes. We present the results of the first nonlinear, two-dimensional, magnetohydrodynamic (MHD) simulation of the magnetosonic waves in plumes for typical coronal conditions consistent with observations and gravitationally stratified solar corona. We find numerically that outward-propagating slow magnetosonic waves are trapped, and nonlinearly steepen in the polar plumes. The nonlinear steepening of the magnetosonic waves may contribute significantly to the heating of the lower corona by compressive dissipation.

Subject headings: MHD — Sun: corona — Sun: magnetic fields — waves

1. INTRODUCTION

Polar plumes are cool, dense, linear, magnetically open structures that arise from predominantly unipolar magnetic footpoints in the solar polar coronal holes, subtending roughly 2° relative to the Sun center at low altitude and expanding superradially with the coronal hole (Newkirk & Harvey 1968).

With topologically simple structure and little impulsive activity, they are among the more quiescent features found in the lower solar corona. Because of their relative simplicity, learning about polar plumes' heating and acceleration mechanisms is important to understanding the "background" processes that heat the coronal hole regions and accelerate the solar wind.

The Extreme-Ultraviolet Imaging Telescope (EIT) (Delaboudinière et al. 1995), with its relatively high exposure rate, signal-to-noise ratio, and resolution, provides a new window into plume activity on timescales of a few minutes and spatial scales of a few arcseconds.

Karovska et al. (1994) claim to have seen filamentary structure in polar plumes with *Skylab* data; and work by Withbroe (1983) has provided evidence that plumes fluctuate in brightness by ~10% on timescales of a few minutes. The high quality of the EIT data makes possible considerable advances in both these areas.

Previous plume models have generally assumed a one-dimensional model for each plume and have neglected time dependence and waves (e.g., Walker et al. 1993; Wang 1994). More elaborate models did not include the effects of waves (e.g., Del Zanna, Hood, & Longbottom 1997). Ofman & Davila (1995) investigated the heating of polar plumes that results from the dissipation of Alfvén waves in the plume boundary inhomogeneities. They used linear two-dimensional model and neglected the effect of gravity and sound waves. Nakariakov & Roberts (1995) considered various mechanisms for the trapping of magnetosonic waves in transversally structured media. In particular, they show that the transverse structure, such as discussed in the present paper in the context of plumes, is a waveguide for fast and slow body magnetosonic waves.

Here we reanalyze the EIT plume observation and show for the first time that the relative wave amplitude increases with height. We study the propagation of trapped slow magnetosonic waves in plumes using the one-dimensional linear wave equation and a nonlinear two-dimensional magnetohydrodynamic (MHD) code in spherical geometry, and find good agreement with observations. This is the first two-dimensional MHD study of the propagation of slow magnetosonic waves in plumes in the linear and nonlinear regimes.

2. RECENT OBSERVATIONS OF WAVES IN POLAR PLUMES

Recently, DeForest & Gurman (1998) demonstrated that there is filamentary structure within plumes, on a spatial scale of 3″–5″, changing on a timescale of a few to ten minutes, and that there are coherent outwardly propagating brightness structures that propagate at ~75–150 km s^{-1} and recur quasi-periodically on timescales of ~10 minutes.

Recent observations by Ofman et al. (1997) of coronal holes using the white-light channel (WLC) of the Ultraviolet Coronagraph Spectrometer (UVCS) report density fluctuations on a timescale of 9.3 ± 0.4 minutes (see, e.g., Ofman et al. 1998). The WLC may have detected the compressional waves observed by EIT farther out in the corona, at 1.9 $R_\odot$.

The EIT observations on 1996 March 7 included a sequence of 104 frames, spaced at <3 minute intervals, of the south polar coronal hole in the 171 Å (Fe IX and X) passband. The exposure time was 7 s. The radial background model corona was subtracted from each EIT frame. Several bright plumes were observed during the mini-

campaign, typically extending from the base of the corona to $\sim 1.3\ R_\odot$ before fading into the background noise. The plumes remained relatively constant in overall 171 Å brightness for periods of up to several hr. However, movies made from the sequence were observed to have a wavering, "ripply" appearance, hinting that small-scale motions might be occurring.

Six of the brightest plumes and one nonplume region that were selected for analysis are shown in Figure 1 (*top*). The three bottom panels in Figure 1 show plume 2 (with another plume visible in the background) as seen in three frames of the sequence. The pictured frames are separated by 9 minutes (i.e., three frames), and have been background subtracted to increase contrast. Each of the two pictured plumes shows distinct filamentary structures within its core. The filamentary structures change their overall shape dramatically during the 9 minutes between each of the images in Figure 1.

To identify coherent motions along the plumes, DeForest & Gurman (1998) generated synoptic-like maps of the evolution of each plume's core, using the derotated sequences of subfields. They extracted a vertical strip of the middle few pixels of each image, and laid the strips side-by-side to produce a time-evolution chart of the plume's brightness. Finally, to emphasize only the time-variable aspects of the plumes' behavior, DeForest & Gurman (1998) subjected each evolution chart to a running-difference process: each frame had the subfield from 6 minutes prior subtracted from it. They found traveling features in the 75–150 km s^{-1} range by measuring the slope in the evolution map.

In Figure 2 we show the relative (to the background intensity) wave amplitude dependence on the height in plume 4 and the background-intensity dependence on the height. The background-subtracted line-of-sight intensity of the plume is proportional to the square of the plume density (since the radiation is due to line emission). The relative intensity is proportional to the relative density variations. Note that the exponential decrease in the intensity of the plume is in agreement with gravitational stratification of the density. The increase of the relative wave amplitude is in good agreement with the linear theory and the two-dimensional MHD simulations (see §§ 3 and 4 below). A similar increase in the relative wave amplitude was also observed in plumes 5 and 6. There was a less evident increase of the relative wave amplitude in plumes 1, 2, and 3, due to the presence of more than one bright plume in the line of sight, and no significant increase in the control case (plume 0).

The amplitudes of the waves were calculated as follows. For each location in the plume, a $5'' \times 5''$ area (see the plume image in Fig. 2) was used to accumulate a time series of the background-subtracted intensity. The background

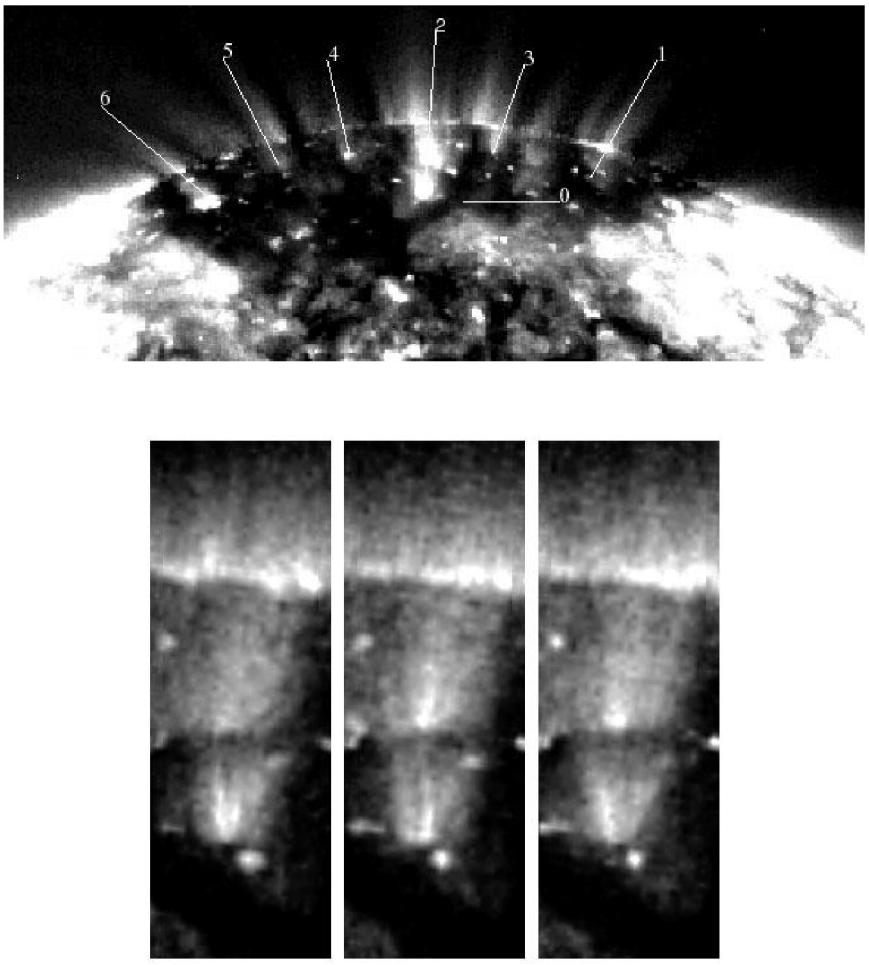

FIG. 1.—Polar plumes over the south pole of the Sun as seen in the EIT 171 Å on 1996 March 7 (*top*). A radial background model of the corona has been subtracted from this image. Three views of plume 2 are seen, taken 9 minutes apart, with two plumes visible (*bottom*). The width of the frames is about 6×10^9 cm on the Sun. Note the changes in brightness and overall structure of each plume between adjacent frames.

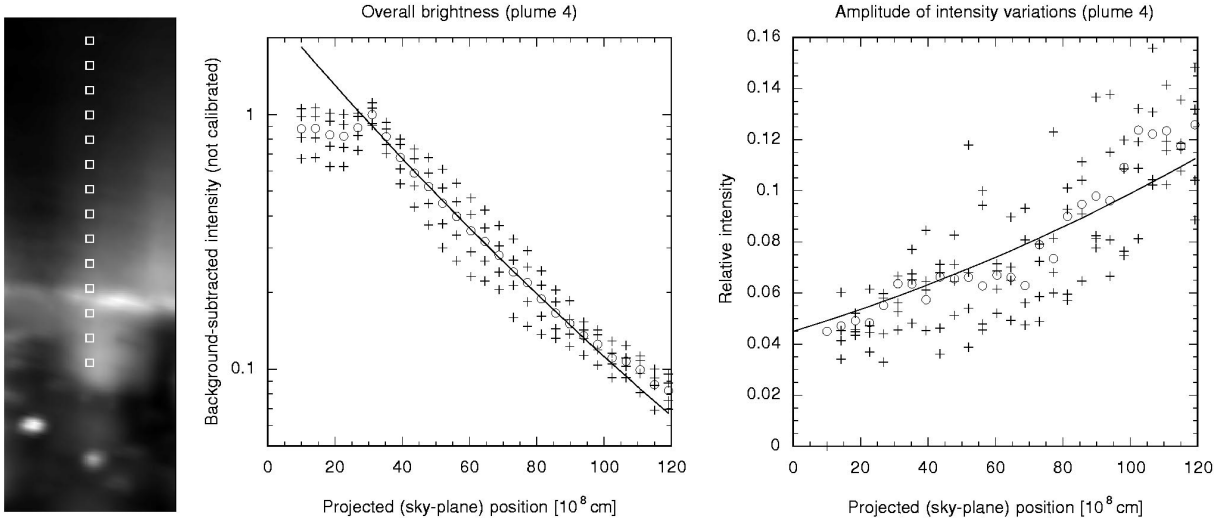

FIG. 2.—*Left*: Background-subtracted intensity dependence on the height in plume 4. *Middle and Right*: Wave amplitude (relative to the background intensity) dependence on the height in plume 4. The data are plotted by circles; estimates of the upper and the lower limits (see text) are marked by crosses. The solid line in the middle panel shows a scale-height fit in the position range 35–90 $\times$ 10^8 cm made using eq. (6). The solid line in the right panel shows the fit of the analytical relative wave amplitude (eq. [7]) with the scale height obtained from the left panel fit. Note the good agreement between the observed and analytical increases of the relative wave amplitude with height. The locations of the observations in the plume are marked by squares in the plume image.

coronal intensity was calculated as in DeForest & Gurman (1998). The time series was smoothed with a 40 minute kernel, and the smoothed series was subtracted from the original, so that gradual plume brightness variations would not be counted as extra wave amplitude. Then the rms wave amplitude was calculated and divided by the time average of the smoothed brightness; these amplitudes are plotted as circles. To estimate the uncertainty in the wave amplitude, we broke the time series into four equal parts and reran the complete calculation on each of the four parts for each location in the plume image; these amplitudes are plotted as small crosses. An additional source of uncertainty is the statistical fluctuation in the number of photons measured by the detector (i.e., "shot noise"). This effect contributes 20%–30% to the increase in the relative intensity variations above $\sim 80 \times 10^8$ cm in Figure 2.

3. ANALYTICAL ONE-DIMENSIONAL MODEL OF LINEAR MAGNETOSONIC WAVES IN PLUMES

From observations, the waves are compressive, perturbing the density, and the speed of propagation is 75–150 km s^{-1}, which is slightly less than the sound speed. Consequently, the waves can be interpreted as slow magnetosonic waves. The observed amplitudes of the waves are 10%–20% of the background density value, and consequently the application of a linear model seems to be justified.

The observed wave periods are in the 10–15 minute range. To test whether the corresponding wave frequency is above the acoustic cutoff frequency, we calculate

$$\omega_{\rm cutoff} = \frac{\gamma g}{2C_s} ; \qquad (1)$$

with adiabatic index $\gamma = 5/3$, gravity acceleration $g = 27{,}400$ cm s^{-2}, and sound speed $C_s = 152$ km s^{-1} for $T = 10^6$ K, we obtain $\omega_{\rm cutoff} \approx 1.5 \times 10^{-3}$ rad s^{-1}. Consequently, waves with periods over 70 minutes are evanescent. Thus, the periods of the observed waves are much shorter and the waves are propagating into the corona.

For wave periods of about 10 minutes and wave speeds of 100–150 km s^{-1}, the wavelength is 6–9 $\times$ 10^9 cm. The wavelength is not much larger that the plume cross section (3–4 $\times$ 10^9 cm) at the height of observation; consequently, since the characteristic spatial scale of the waves is of the same order as the spatial scale of the inhomogeneity, and the waves are observed close to the level of their excitation, they seem to be described by the one-dimensional model, at least at the plume axis. However, trapping effects are important, and will be discussed in the following section.

Consider linear one-dimensional dynamics of slow magnetosonic waves propagating along the vertical magnetic field. The magnetic field is taken to be radially divergent. The atmosphere is spherically stratified by gravity, with the equilibrium density given by

$$\rho_0 = \rho_{00} \exp\left[-\frac{R_\odot}{H}\left(1 - \frac{R_\odot}{r}\right)\right], \qquad (2)$$

where $R_\odot$ is the solar radius and H is the scale height, defined as $H = 2k_{\rm B}TR_\odot^2/(GM_\odot m_{\rm H})$ where $k_{\rm B}$ is Boltzmann's constant, T is the temperature, G is the gravitational constant, $M_\odot$ is the Sun's mass, and $m_{\rm H}$ is the hydrogen mass. The scale height can be estimated as $H(10^8$ cm$) \approx 61T(10^6$ K) (where the factor in front of T is 51 when Helium is taken into account).

In spherical coordinates, the linear spherical slow magnetosonic waves radially propagating strictly along the magnetic field contain perturbations of plasma density ρ and radial speed V_r that are governed by the equations

$$\frac{\partial \rho}{\partial t} + \frac{1}{r^2}\frac{\partial}{\partial r}(r^2 \rho_0 V_r) = 0 , \qquad (3)$$

$$\rho_0 \frac{\partial V_r}{\partial t} + C_s^2 \frac{\partial \rho}{\partial r} + g\rho = 0 , \qquad (4)$$

where $g = GM_\odot/r^2$ is the gravity acceleration. Perturbations of the magnetic field and transverse components of

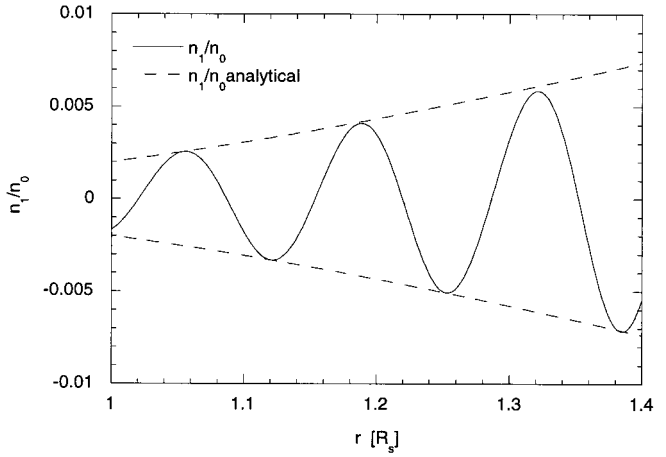

FIG. 3.—Radial dependence of the relative density fluctuation, n_1/n_0 (*solid line*) obtained from the numerical solution of the MHD equations. The amplitude of $\pm n_1/n_0$ has been obtained from eq. (7). Note the excellent agreement between the numerical and the analytical solutions. Parameters are $T = 10^6$ K, $n_{10} = 0.002$.

the plasma velocity are not excited by the linear radially propagating slow wave considered here.

Equations (3) and (4) can be combined into the wave equation

$$\frac{\partial^2 \rho}{\partial t^2} - \frac{C_S^2}{r^2}\frac{\partial}{\partial r}\left(r^2 \frac{\partial \rho}{\partial r}\right) - g\frac{\partial \rho}{\partial r} = 0\,, \tag{5}$$

with the approximate solution (e.g., Torkelsson & Boynton 1998)

$$\rho \sim \frac{R_\odot}{r} \exp\left[-\frac{R_\odot}{2H}\left(1 - \frac{R_\odot}{r}\right)\right]. \tag{6}$$

Equation (6) shows that the absolute amplitude of the density perturbations decreases with height, while the ratio of the density perturbation amplitude (eq. [6]) and the local equilibrium density value grows,

$$\frac{\rho}{\rho_0} \sim \frac{R_\odot}{r} \exp\left[\frac{R_\odot}{2H}\left(1 - \frac{R_\odot}{r}\right)\right]. \tag{7}$$

In the isothermal atmosphere, the growth rate of the ratio ρ/ρ_0 depends on the temperature T only. In the presence of dissipative processes, the dissipation rate should be subtracted from the growth rate.

In Figure 3 we show the radial dependence of the relative density fluctuation, $\rho/\rho_0 = n_1/n_0$ (*solid line*) obtained from the numerical solution of the two-dimensional MHD equations (see below), with the density perturbation amplitude $n_{10} = 0.002$ and $T = 10^6$ K, for the one-dimensional case. The small value of n_{10} ensures that the MHD solution is in the linear regime. The amplitude of $\pm n_1/n_0$ obtained from equation (7) is plotted with dashed lines. Note the excellent agreement between the numerical and analytical solutions.

We find that the increase in the relative slow magnetosonic wave amplitude with height is in good agreement with the observations. The solid line in the middle panel of Figure 2 is a scale-height fit in the position range 35–90 $\times$ 10^8 cm (where the scale height is nearly constant and corresponds to $T \approx 10^6$ K), using equation (2). The solid line in the right panel is the fit of the analytical relative wave amplitude (eq. [7]), using the scale height obtained from the left panel fit. In the above calculations, the small projection effects are not taken into account.

4. NUMERICAL TWO-DIMENSIONAL MHD MODEL OF THE MAGNETOSONIC WAVES IN POLAR PLUMES

The slow magnetosonic waves reduce to sound waves in the case of purely longitudinal propagation in a one-dimensional medium. Thus, § 3 dealt with sound waves. However, when transverse structure of the medium is present in a more realistic model of a plume, the waves have a transverse wavenumber. Nakariakov & Roberts (1995) show that the structure discussed in the present paper is a waveguide for fast- and slow-body magnetosonic waves. Qualitatively, trapping of magnetosonic waves may occur when a transversely structured medium (a tube or a slab) acts as a waveguide as a result of differences in magnetosonic speeds inside and outside the medium. For a plane slab approximating the plume model given below, the trapping will occur for slow magnetosonic waves traveling slightly below the sonic ($\approx$tube) speed. The exact conditions for trapping magnetosonic waves in a plane slab can be found in Nakariakov & Roberts (1995).

When gravity, magnetic field, and nonlinearity are included together with transverse structure, the problem of magnetosonic waves in plumes is intractable analytically, and the two-dimensional MHD equations are solved numerically. The main goal of the numerical simulation of the slow magnetosonic waves in plumes is to investigate the roles of plume structure and nonlinearity in the propagation of the waves. For this purpose, we model the polar plume in the r-θ plane with a two-dimensional MHD nonlinear code in spherical geometry, where r lies along the solar radial direction ($r = 1$ is the coronal boundary), and θ is the latitudinal direction. We include resistive dissipation and a polytropic energy equation. In this preliminary study, we neglect background flow and viscous dissipation, assume $\partial/\partial\phi = 0$, and set the polytropic index to be $\gamma = 1$. We plan to relax some of the above assumptions in our future studies.

The normalized MHD equations are

$$\frac{\partial \rho}{\partial t} + \nabla \cdot (\rho \boldsymbol{v}) = 0\,, \tag{8}$$

$$\frac{\partial \boldsymbol{v}}{\partial t} + (\boldsymbol{v} \cdot \nabla)\boldsymbol{v} = -\frac{E_u}{\rho}\nabla p - \frac{1}{F_r r^2} + \frac{\boldsymbol{J} \times \boldsymbol{B}}{\rho}\,, \tag{9}$$

$$\frac{\partial \boldsymbol{B}}{\partial t} = \nabla \times (\boldsymbol{v} \times \boldsymbol{B}) + S^{-1}\nabla^2 \boldsymbol{B}\,, \tag{10}$$

$$\left(\frac{\partial}{\partial t} + \boldsymbol{v} \cdot \nabla\right)\frac{p}{\rho^\gamma} = 0\,. \tag{11}$$

The quantities in the MHD equations are normalized with $r \to r/R_\odot$, $t \to t/\tau_A$, $v \to v/v_A$, $B \to B/B_0$, $\rho \to \rho/\rho_0$, and $p \to p/p_0$. The physical parameters are the Lundquist number, $S = \tau_r/\tau_A$; the resistive timescale, $\tau_r = 4\pi R_\odot^2/\nu c^2$, where ν is the resistivity and c is the light speed; the Alfvén timescale, $\tau_A = R_\odot/v_A$; the Froude number, $F_r = v_A^2 R_\odot/(GM_\odot)$; the Euler number, $E_u = p_0/(\rho_0 v_A^2) = C_s^2/v_A^2$ ($\equiv \beta/2$); and the sound speed, $C_s = (\gamma p_0/\rho_0)^{1/2}$. The values of the magnetic field B_0, pressure p_0, and density ρ_0 are taken at the solar boundary of the plumes.

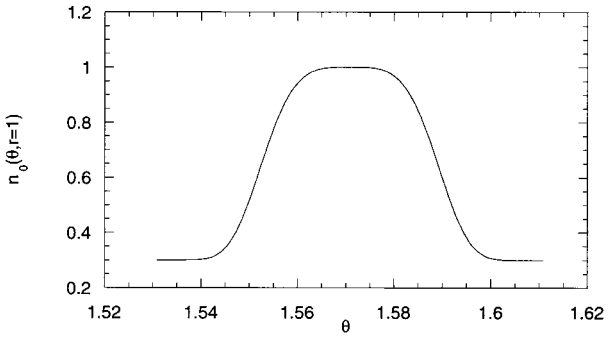

FIG. 4.—θ-dependence of the initial normalized density in the plume at $r = 1$.

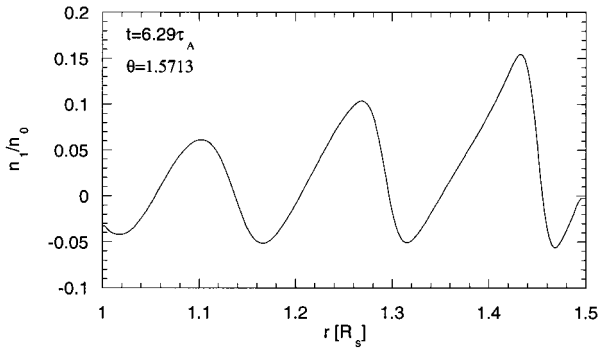

FIG. 6.—Radial variation of n_1/n_0 in the plume due to the propagating magnetosonic wave. The nonlinear steepening of the wave is evident.

The simulations are initiated with the normalized number density profile that represent the polar plume

$$n_0(\theta, r) = [n_{\min} + (1 - n_{\min})e^{-(\theta/d)^8}]e^{-\alpha[1-(1/r)]}, \quad (12)$$

where d is the normalized plume half-width, $n_{\min} = 0.3$ is the normalized density of the surrounding coronal hole, with the normalization $n_0(1) = 1$ at the center of the plume, and $\alpha = (E_u F_r)^{-1} = R_\odot/H$ is the normalized inverse scale height. The θ-dependence of n_0 is shown in Figure 4. In the uniform magnetic field, such density structure is a wave-

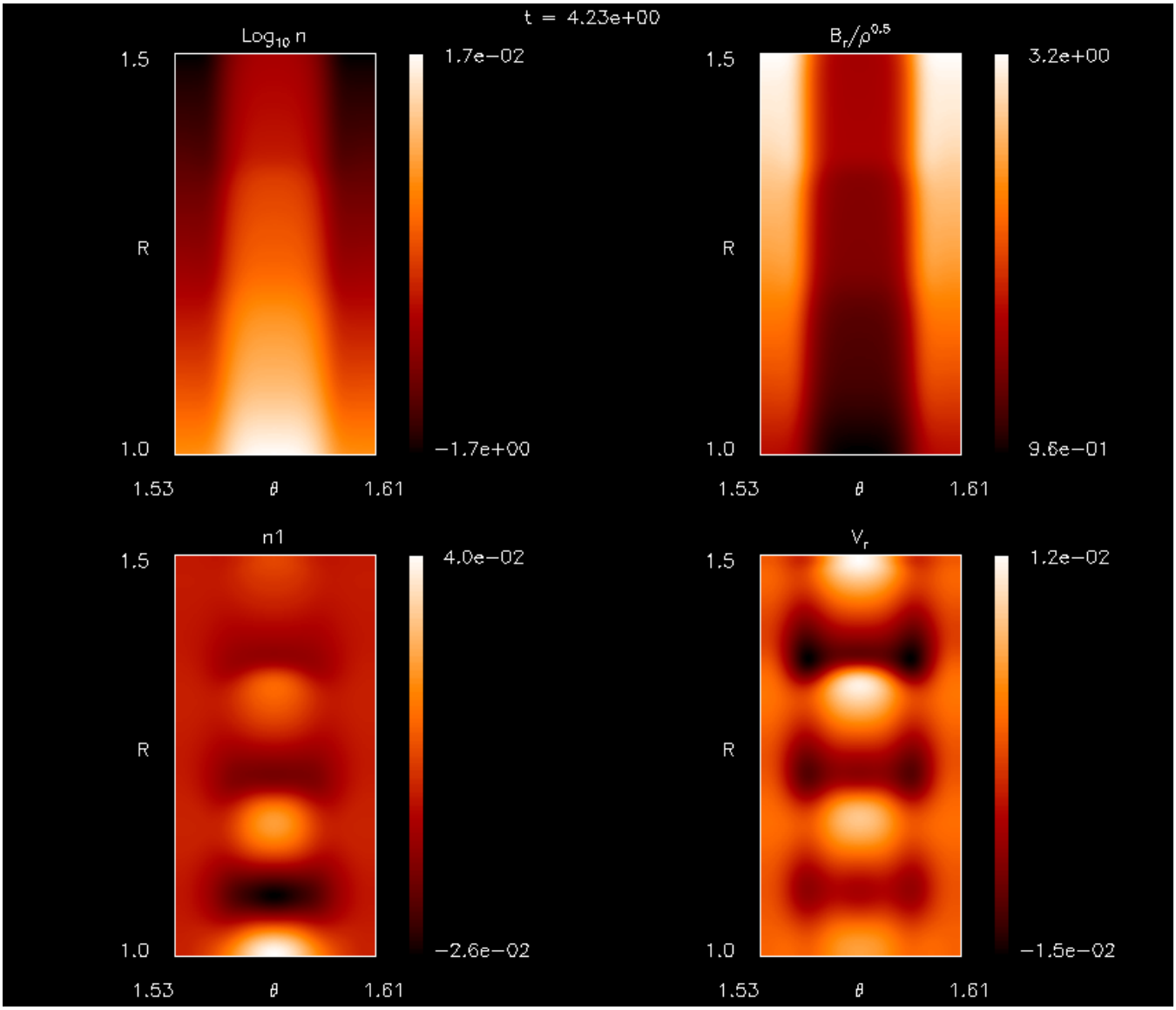

FIG. 5.—Snapshot at $t = 4.23\tau_A = 39$ minutes of the spatial variations of the density n, the perturbed density n_1, the v_r, and the B_r due to the propagating magnetosonic waves in the polar plume.

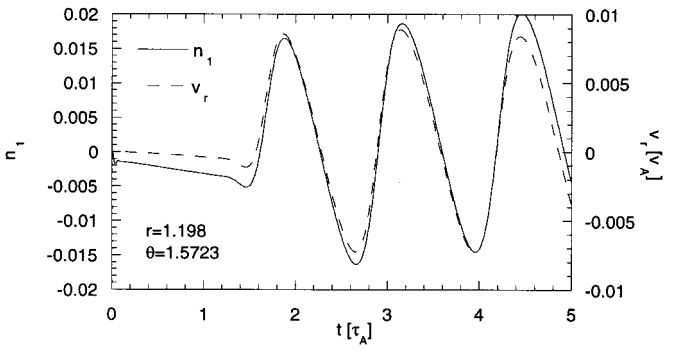

FIG. 7.—Temporal variations in the plume at $r = 1.198$, $\theta = 1.5723$ due to the propagating magnetosonic wave.

guide for trapped fast and slow magnetoacoustic waves. The radial dependence is given by gravitational hydrostatic equilibrium.

The initial magnetic field $\boldsymbol{B} = B_0(r)\boldsymbol{e}_r$ is uniform in the θ-direction and varies as $1/r^2$. We use the following typical coronal hole parameters in our run: $n_{00} = 3 \times 10^8$ cm^{-3}, $B_0 = 10$ G, $v_A = 1259$ km s^{-1}, $\tau_A = 556$ s, and we set $S = 10^6$. Guhathakurta, Fisher, & Strong (1996) report line ratio (i.e., electron) temperatures in plumes in the range of 0.7–1.3 $\times 10^6$ K at 1.15 $R_\odot$. We use $T = 1.4 \times 10^6$ K in our two-dimensional model. This temperature is higher than the electron temperature in plumes. However, in a single-fluid MHD model, the temperature reflects the combined effects of electrons, protons, alpha particles, and heavier elements on the thermal pressure, and is consistent with the scale-height temperature observed in plumes (see Table 1 in Walker et al. 1993). With the above parameters, we get $E_u = 0.0145739$ and $F_r = 8.36114$.

For the upper boundary of the plumes and at the θ-boundaries, we use open boundary conditions. We allow for incoming characteristics at the solar boundary by using zero-order extrapolation for the variables (e.g., Steinolfson & Nakagawa 1976). The density perturbation $n_1(\theta, r = 1, t)$ is driven harmonically with $\omega = 4.84\tau_A^{-1}$ and an amplitude of $n_{10} = 0.04$:

$$n_1(\theta, r = 1, t) = n_{10}\, e^{-(\theta/d)^2} \sin \omega t\,, \qquad (13)$$

where $d = 0.02$ $R_\odot$. The magnetosonic waves that are excited with the above driver are not coupled to Alfvénic fluctuations, since $\partial/\partial\phi = 0$. Thus, v_ϕ and B_ϕ remain zero throughout the simulation in the plume.

We solve the two-dimensional MHD equations using a fourth-order Runge-Kutta method in time, with fourth-order spatial differencing at 80 $\times$ 200 grid points. Figure 5 shows a snapshot at $t = 4.23\tau_A = 39$ minutes of the spatial variations of the density n, the perturbed density n_1, the v_r, and the nonlinearly perturbed B_r due to the propagating magnetosonic waves in a high-density, low-temperature (compared to the surrounding corona) polar plume.

The spatial variation in the perturbed quantities n_1 and v_r are in phase, as expected from the linear theory of traveling waves. It is evident in Figure 5 that the plume width affects the shape of the waves and leads to trapping of the waves. However, small-amplitude magnetosonic waves can be detected outside the plume. This could be due to the energy contained in the tails of the Gaussian shape driver (eq. [13]) and a small leakage of the wave energy outside the plume, or evanescent tails of the trapped modes.

The amplitude of the waves is small ($n_1/n_0 \ll 1$), and the solution is in the nearly linear regime near the solar surface. As the magnetosonic waves propagate outward, the quantity n_1/n_0 increases, and the nonlinear steepening of the waves becomes apparent (see Fig. 6). The possible formation of shocks at larger distances will be determined by the balance between nonlinear steepening and the dissipative and dispersive effects (e.g., Ofman & Davila 1997, 1998). The steepening of the waves and the formation of shocks will lead to enhanced viscous dissipation of the wave energy and heating of the plumes.

In Figure 7 we show the temporal variation of v_r and n_1 at $r = 1.198$ $R_\odot$, $\theta = 1.5723$ (i.e., near the central axis of the plume). It is evident that the modeled density and velocity fluctuations of the traveling waves are in phase, as expected from the linear theory. Because of the time it takes for the magnetosonic wave to reach 1.198 $R_\odot$, there is no significant variation in n_1 and v_r in the first $1.5\tau_A$. The amplitude of the waves is small, and the solution is in the nearly linear regime, with some nonlinear steepening evident. The nonlinear steepening leads to an asymmetry in the shape of the waves. Nonlinearity also modifies the initial hydrostatic background equilibrium and leads to changes in the wave amplitude with time.

The phase speed, the amplitude, and the frequency of the waves are in qualitative agreement with recent observations of waves in plumes by DeForest & Gurman (1998). The observed relative wave amplitude with height shows an increase in qualitative agreement with the increase of n_1/n_0 with r in the numerical and analytical plume models. The agreement between the analytical, numerical, and observational properties of the waves strongly suggests that the observed waves are slow magnetosonic waves propagating in the plumes.

5. DISCUSSION AND CONCLUSION

High-cadence *SOHO*/EIT observations indicate that quasi-periodic fluctuations with periods of 10–15 minutes are present in polar plumes. The fluctuations were found to propagate outward in the plumes at speeds of 75–150 km s^{-1} (DeForest & Gurman 1998). By performing additional analysis of the 1996 March 7 plume observations, we found that the relative wave amplitude increases with height in the plumes to about 1.2 $R_\odot$ (beyond this height the signal-to-noise ratio becomes too small). The observations suggest that slow magnetosonic waves propagate in plumes.

The energy flux carried by the slow magnetosonic waves can be estimated as $\rho[(\delta v)^2/2]v_s$, where δv is the wave velocity amplitude, and $v_s \approx c_s = 150$ km s^{-1} in the low-β coronal plasma. Using $\rho = 5 \times 10^{16}$ g cm^{-3} and $\delta v = 7.5$ km s^{-1}, we get the wave energy flux $\sim 2 \times 10^3$ ergs cm^{-2} s^{-1}. Note that in DeForest & Gurman (1998), the wave energy flux was overestimated due to computational error. Using their parameters ($\rho = 1.67 \times 10^{-15}$ g cm^{-3} and $\delta v = 15$ km s^{-1}), we get 2.8×10^4 ergs cm^{-2} s^{-1} as the upper bound for the wave energy flux. This energy is a significant fraction of the total energy required to accelerate the fast solar wind ($\sim 10^5$ ergs cm^{-2} s^{-1}).

The exact reason for the 10–15 minute periodicity is not know. It appears that the waves are generated below the corona and could be the result of direct driving of 10–15 minute perturbation by photospheric motions or some nonlinear transformation of the solar 5 minute oscillation in the transition region. The first hypothesis could be tested by

observing the spectrum of the photospheric motions below the plumes. The second hypothesis could be tested by spectral observations and modeling of the wave propagation and steepening in the chromosphere and the transition region. We hope that the answer to this question will emerge in the near future from *SOHO* observations and models.

We obtain analytical solutions for the propagation of the magnetosonic waves in a gravitationally stratified, linear, one-dimensional model of the polar plumes. We find that for typical coronal conditions, 10–15 minute waves are propagating in the plume. Waves with periods longer than 70 minutes will become evanescent. We find that the observed wave amplitude increases with height, in good agreement with the model predictions.

We investigate the effects of the plume structure and nonlinearity on the propagation of the magnetosonic waves using the two-dimensional MHD model. We further establish that the observed fluctuations are slow magnetosonic waves that propagate in the plumes. The propagation speed for these waves is close to the sound speed in the low-β plasma ($C_s \ll v_A$). We find that the slow magnetosonic waves nonlinearly steepen with height. The steepening may lead to the formation of shocks higher in the corona, and may contribute significantly to the solar-wind acceleration by transferring momentum to the flow, and to heating by viscous dissipation. We plan to investigate the dissipation of these waves in a future paper.

We would like to thank Joseph M. Davila, Bernard Roberts, and Madhulika Guhathakurta for insightful discussions, and the referee for his comments that helped to improve this paper. Part of this work was supported by NASA grant 879-11-38, the NASA *SOHO* Guest Investigator program, the NASA Space Physics Theory program, and the NASA HPCC Program. Craig DeForest is supported by NASA grant NAG5-3077. *SOHO* is a project of international collaboration between NASA and ESA.

REFERENCES

DeForest, C. E., & Gurman, J. B. 1998, ApJ, 501, L217
Delaboudinière, J.-P., et al. 1995, Sol. Phys., 162, 291
Del Zanna, L., Hood, A. W., & Longbottom, A. W. 1997, A&A, 318, 963
Guhathakurta, M., Fisher, R., & Strong, K. 1996, ApJ, 471, L69
Karovska, M., et al. 1994, ApJ, 428, 854
Nakariakov, V. M., & Roberts, B. 1995, Sol. Phys., 159, 213
Newkirk, G., Jr., & Harvey, J. 1968, Sol. Phys., 3, 321
Ofman, L., & Davila, J. M. 1995, J. Geophys. Res., 100, 23413
———. 1997, ApJ, 476, 357
———. 1998, J. Geophys. Res., 103, 23677
Ofman, L., Romoli, M., Poletto, G., Noci, G., & Kohl, J. L. 1997, ApJ, 491, L111
———. 1998, ApJ, 507, L189
Steinolfson, R. S., & Nakagawa, Y. 1976, ApJ, 207, 300
Torkelsson, U., & Boynton, G. C. 1998, MNRAS, 295, 55
Walker, A. B. C., DeForest, C. E., Hoover, R. B., & Barbee, T. W. 1993, Sol. Phys., 148, 239
Wang, Y.-M. 1994, ApJ, 435, L153
Withbroe, G. L. 1983, Sol. Phys., 89, 77